Astron. Astrophys. 318, 963–969 (1997)

ASTRONOMY
AND
ASTROPHYSICS

An MHD model for solar coronal plumes

L. Del Zanna, A.W. Hood, and A.W. Longbottom

Mathematical Sciences Department, University of St. Andrews, St. Andrews, KY16 9SS, UK

Received 29 May 1996 / Accepted 22 July 1996

Abstract. Solar coronal plumes are modelled by solving the steady, ideal, 2-D, magnetohydrodynamic (MHD) equations and assuming azimuthal symmetry around the plume axis. Since magnetic fields are believed to play an essential role in plume formation and structure, a self-consistent method of linearisation of the MHD equations with respect to the magnetic field has been considered here. This consists of three distinct steps: first a potential field is calculated as a deviation from the radial case due to a flux concentration at the plume base, then the other plasma quantities are worked out by solving a Bernoulli-like equation and finally the modifications to the zeroth order field are found. Free functions of the model are the radial field component at the coronal base, the density at the coronal base and the temperature, which is assumed to be constant along the field lines. This method allows one to reproduce basic features of coronal plumes such as the super-radial expansion close to their base. The results are compared with the observations.

Key words: MHD – Sun: corona – Sun: magnetic fields – solar wind – stars: coronae – stars: magnetic fields

1. Introduction

Solar coronal plumes were first observed in white light eclipse photographs as long, faint rays of enhanced density (3 – 5 times denser than the background) located inside coronal holes (e.g. Van de Hulst, 1950; Saito, 1965; Koutchmy, 1977). In extreme ultraviolet (EUV) spectroheliograms they appear as shorter spikes near the polar limb (Bohlin et al., 1975; Ahmad & Withbroe, 1977; Widing & Feldman, 1992; Walker et al., 1993) and they show lifetimes of several hours or even days. Recently, diffuse Mg IX plume-like structures have been observed inside low-latitude coronal holes undergoing limb passage (Wang & Sheeley, 1995a), thus suggesting that coronal plumes are common features of all coronal hole regions and not only in the polar caps (therefore the term *coronal* plume should be preferred to *polar* plume, although the latter is more commonly used). Plumes have been also identified in soft X-ray images (Ahmad & Webb, 1978) and possibly even as weak radio sources (Gopalswamy et al., 1992). More recently, white light observations by the *Spartan* spacecraft coronograph, up to a height of 5 solar radii, have been analysed by Fisher & Guhathakurta (1995).

Characteristic values of coronal plumes, as seen at the solar limb, are widths of $6-7\times10^4$ km, number densities in the range $10^8 - 10^9\,\mathrm{cm}^{-3}$ and temperatures around 10^6 K (Mg IX lines, where plumes intensities peak, form around 9.5×10^6 K). The outflow velocity is unknown, but it should not be larger than, say, $10\,\mathrm{km\,s}^{-1}$ at the base of the plume (plumes are observed to be roughly in hydrostatic equilibrium), thus suggesting that the bulk of the solar wind acceleration occurs at larger heights. Finally, no measures of the magnetic field are available, although usual coronal values for the plasma beta ($\approx 1\%$) are commonly assumed.

Together with macrospicules, short-lived ($\sim$ 30 minutes) jets of cooler chromospheric material, coronal plumes are believed to trace the open field lines structure and to provide a major source of the solar wind. Possible remnants of the signature of these coronal hole fine structures have been discovered (Thieme et al., 1990) by analysing high-speed streams data taken by the *Helios* probes in the range 0.3 – 1 AU. Their results show that plumes expand while retaining an overall pressure balance with the background, thus suggesting that the magnetic field open lines play an important role in confining the plume plasma even in the outer corona. This behaviour has been investigated by Velli et al. (1994), who proposed an interesting thin flux-tube model in which the magnetic flux is conserved separately both in the plume and in the surrounding coronal hole and total pressure is balanced across the field lines.

Another fundamental observational result, confirming the intrinsic magnetic nature of coronal plumes, is the connection between plumes and magnetic surface features related with flux concentrations. Before the *Skylab* era plumes were believed to be rooted in unipolar flux concentrations in relation with photospheric or chromospheric faculae, located at the vertices between supergranular cells (Newkirk & Harvey, 1968). This picture was supported by the coincidence of the mean plume separation ($\approx 7\times10^4$ km) and the size of a typical supergranular cell. After the discovery of the presence of compact EUV enhancements at the base of the most bright plumes (Bohlin et al., 1975), which in turn correspond to X-ray bright points, the attention has shifted towards magnetic bipolar regions (Golub et al., 1974; Habbal, 1992; Dowdy, 1993). These observations

Send offprint requests to: L. Del Zanna

have suggested a possible explanation for plumes formation: one or more bipoles are pushed by photospheric motions towards an open flux region located at a supergranular junction; eventually reconnection occurs, field lines open up and the required energy for plume formation is released. This mechanism has been analysed in more detail by Wang & Sheeley (1995b), whereas a systematic analysis of the effect of heating of the inner corona at the plume base may be found in Wang (1994), who also investigated the solar wind implications by solving the full energy equation along the radial direction (although pressure balance across the field lines is not taken into account).

However, so far there is little direct evidence for the relationship between plumes and network activity (magnetograms cannot be taken at the limb, where the plumes are more easily observable), though anyway it seems reasonable to assume that plumes are rooted in open flux concentration regions. In support of this idea come the observations of a super-radial expansion of plumes near their base, say in the range $1 - 1.2\,R_\odot$ (Saito, 1965; Ahmad & Withbroe, 1977; Ahmad & Webb, 1978). What is observed is obviously a density behaviour, but if the plume is to be in equilibrium, then it must be threaded by diverging field lines with increasing height (Ahmad & Withbroe, 1977). Potential field models trying to explain this behaviour were proposed by Newkirk & Harvey (1968) and by Suess (1982), but none of them include the plasma parameters in their analysis. Suess's model consists of an analytical, two dimensional field in Cartesian geometry with a given vertical field at the plume base. A comparison with the results by Ahmad & Withbroe is also made, but unfortunately the whole analysis is affected by a trivial mistake (a factor π missing in the decaying exponential function of height).

The main goal of the present paper is to present a self-consistent MHD model which correctly reproduces the observed super-radial expansion near the plume base, assuming that magnetic effects are dominant in the inner corona but taking into account the pressure, inertial and gravity forces as well. This will be achieved by solving the steady, ideal, 2-D MHD equations linearised with respect to the magnetic field under the assumption of a low-beta coronal plasma. The method of solution and the general equations are presented in Sect. 2, whereas the actual plume model is discussed in Sect. 3, first in the simple radial case and then assuming a flux concentration at the base of the plume.

2. Low-beta, 2-D equilibria: basic equations in spherical geometry

The steady, ideal MHD equations may be written in the non-dimensional form:

$$\nabla \cdot \boldsymbol{B} = 0, \tag{1}$$

$$\nabla \cdot (\rho \boldsymbol{V}) = 0, \tag{2}$$

$$\nabla \times (\boldsymbol{V} \times \boldsymbol{B}) = 0, \tag{3}$$

$$(\nabla \times \boldsymbol{B}) \times \boldsymbol{B} = (\beta_\star/2)[M_\star^2 \rho (\boldsymbol{V} \cdot \nabla)\boldsymbol{V} + \nabla P + g_\star \rho r^{-2} \boldsymbol{e}_r], \tag{4}$$

where all the quantities have been non-dimensionalized against typical coronal values and where the values of the three parameters

$$\beta_\star = \frac{8\pi P_\star}{B_\star^2}, \quad M_\star = \frac{V_\star}{V_{s\star}}, \quad g_\star = \frac{GM_\odot m_p}{2kT_\star R_\odot}$$

indicate the relative importance of the various terms in Eq. (4) (here $V_{s\star} = \sqrt{2kT_\star/m_p}$ is a reference value of the sound speed and all the other symbols have their usual meaning).

The main assumption in our model is that the magnetic forces are dominant over all the others, namely pressure gradients, gravity and inertial forces. In the low solar corona this is a good approximation and the coronal plasma is thus regarded as low-β. Hence, in order to linearise the MHD equations with respect to the magnetic field, the following form for $\boldsymbol{B}$ is assumed:

$$\boldsymbol{B} = \boldsymbol{B}_0 + (\beta_\star/2)\boldsymbol{B}_1,$$

where its zeroth order component $\boldsymbol{B}_0$ is necessarily force-free (from Eq. (4)).

Consider now a purely 2-D spherical coordinate system in which all the quantities lie in the r - θ plane and do not depend upon the azimuthal coordinate ϕ (the plume axis will coincide with the symmetry axis $\theta = 0$). Using the formalism of the flux functions, Eqs. (1) to (3) give

$$B_{0r} = \frac{1}{r^2 \sin\theta}\frac{\partial A_0}{\partial \theta}, \quad B_{0\theta} = -\frac{1}{r \sin\theta}\frac{\partial A_0}{\partial r},$$

$$B_{1r} = \frac{1}{r^2 \sin\theta}\frac{\partial A_1}{\partial \theta}, \quad B_{1\theta} = -\frac{1}{r \sin\theta}\frac{\partial A_1}{\partial r},$$

$$V_r = \frac{1}{r^2 \sin\theta}\frac{\Psi(A_0)}{\rho}\frac{\partial A_0}{\partial \theta}, \quad V_\theta = -\frac{1}{r \sin\theta}\frac{\Psi(A_0)}{\rho}\frac{\partial A_0}{\partial r},$$

where the magnetic flux function is $A(r,\theta) = A_0 + (\beta_\star/2)A_1$ and Ψ is a free function of A_0 (note that the velocity and magnetic fields are parallel only at the zeroth order). In order to solve the equations a relation between pressure and density is needed. Here the isothermal case will be assumed, thus

$$\boldsymbol{V} \cdot \nabla T = 0 \Rightarrow P = T(A_0)\rho, \tag{5}$$

where the temperature T is another free function of A_0 (thus T is constant along the field lines). Making use of these assumptions, the component of Eq. (4) across $\boldsymbol{B}_0$ splits into the two *transfield* (or generalised Grad-Shafranov) equations

$$\mathscr{S}(A_0) \equiv \frac{\partial^2 A_0}{\partial r^2} + \frac{\sin\theta}{r^2}\frac{\partial}{\partial\theta}\left(\frac{1}{\sin\theta}\frac{\partial A_0}{\partial\theta}\right) = 0, \tag{6}$$

$$\begin{aligned}\mathscr{S}(A_1) \;=\; & M_\star^2\left[\frac{\Psi}{\rho}\frac{\mathrm{d}\Psi}{\mathrm{d}A_0}|\nabla A_0|^2 - \frac{\Psi^2}{\rho^2}\nabla A_0 \cdot \nabla\rho\right] \\ & -\rho r^2 \sin^2\theta\left[\frac{\mathrm{d}E}{\mathrm{d}A_0} + (1 - \ln\rho)\frac{\mathrm{d}T}{\mathrm{d}A_0}\right],\end{aligned} \tag{7}$$

whereas the component along $\boldsymbol{B}_0$ yields the Bernoulli equation

$$\frac{M_\star^2}{2}\frac{\Psi^2}{\rho^2}\frac{|\nabla A_0|^2}{r^2\sin^2\theta} + T\ln\rho - \frac{g_\star}{r} = E(A_0) \tag{8}$$

and E is the third free function of A_0. For the mathematical demonstrations (in the general case) see Del Zanna & Chiuderi (1996).

The main result of the linearisation of the magnetic field is clearly the decoupling of the transfield and Bernoulli equations. This allows one to solve the problem in three distinct steps:

1. Solve the transfield equation, Eq. (6), for the unperturbed field.
2. Solve the Bernoulli equation, Eq. (8), for the density.
3. Solve the transfield equation, Eq. (7), for the correction to the field.

Clearly, the corrections to the magnetic field must remain small and the condition for this is $A_1 \lesssim A_0$.

The same approach in solving the MHD equations through the magnetic field linearisation has been previously adopted by Surlantzis et al. (1994, 1996) in order to model stationary flows in coronal loops and arcades. As their investigation is only concerned with closed field structures in cartesian and cylindrical coordinates, our analysis may be also considered as an extension to the complementary cases not contemplated in that work.

3. The plume model

As discussed in the introduction, plumes appear to be associated with magnetic field concentrations at the coronal base. In this case the potential unperturbed field could be modelled by solving Eq. (6) with an appropriate boundary condition at $r = 1$. However, observations show that plumes structure is mainly radial from $r \approx 1.2\,R_\odot$ onwards (Fisher & Guhathakurta, 1995), hence the simple radial case will be assumed first as a starting approximation in order to investigate more easily the physical implications of the model. The analysis of the general case will be done in Sect. 3.2, where the resulting plume structure near the coronal base will be compared with observational data.

3.1. The radial case

Consider the zeroth order radial field

$$A_0(\theta) = 1 - \cos\theta \Rightarrow \boldsymbol{B}_0(r) = r^{-2}\boldsymbol{e}_r,$$

in a region around the plume axis $\theta = 0$ (where $A_0 \approx \theta^2/2$). Through the definition of the Mach number

$$M = \frac{V}{V_\mathrm{s}} = \frac{M_\star\Psi}{\sqrt{T}\rho\, r^2},$$

and using the continuity equation to eliminate ρ, the radial derivative of the Bernoulli equation yields (the prime denotes a derivative in respect to r)

$$\left(M - \frac{1}{M}\right)M' = \frac{2}{r} - \frac{g_\star}{Tr^2}. \tag{9}$$

This is simply the famous Parker equation for radial, isothermal winds (Parker, 1958). It is well known that the corresponding phase plane (M, r) contains four different regions depending on the position relative to the sonic point $M = 1$. The only physically relevant solution for the solar wind problem is the one crossing the sonic point with $M' > 0$ (Parker or transonic solution) and eventually connecting via a shock to the interstellar medium. Recently the breeze solutions (i.e. those always subsonic in the phase diagram) have been shown to be unstable (Velli, 1994), thus confirming the necessity of the transonic solution for steady, isothermal outflows.

In the present model the temperature is a function of the field lines, hence the sonic radius $r_\mathrm{sonic} = g_\star/2T$ will be a function of the field lines too. This means that the flow becomes supersonic at different radii for different values of θ. Imposing the transonic condition, the equation for M can be integrated again to give

$$M\exp(-M^2/2) = (B_0/B_{0\mathrm{sonic}})\exp(3/2 - 2r_\mathrm{sonic}/r), \tag{10}$$

where $B_0 = 1/r^2$ is the magnitude of the magnetic field and $B_{0\mathrm{sonic}} = 1/r_\mathrm{sonic}^2$. Notice that, because of the transonic condition, the function $\Psi(A_0)$ must be now derived from Eq. (10) and hence it is no longer free.

The density is related to the Mach number through the Bernoulli equation, which yields

$$\rho = \rho_\mathrm{base}\exp[-(g_\star/T)(1 - 1/r)]\exp(-M^2/2), \tag{11}$$

where the relationship $E = T\ln\rho_\mathrm{base} - g_\star$ has been assumed and where $\rho_\mathrm{base}(A_0)$ gives the density profile at $r = 1$ in the static case (for solar values $M_\mathrm{base} \sim 10^{-3}$, hence the dynamic effects are actually negligible at the base of the corona). Note that for a constant temperature everywhere the Mach number does not depend upon θ (from Eq. (10)) and therefore the density profile across the field lines remains the same at all heights.

In order to investigate the behaviour of the physical quantities in our model, the shapes of the two arbitrary functions $\rho_\mathrm{base}(A_0)$ and $T(A_0)$ have to be chosen. Here the following functional forms will be assumed:

$$\rho_\mathrm{base} = 1 + (\rho^0_\mathrm{base} - 1)\exp(-A_0/A_{0\mathrm{w}}), \tag{12}$$

$$T = 1 + (T^0 - 1)\exp(-A_0/A_{0\mathrm{w}}), \tag{13}$$

where the density (temperature) is considered to be non-dimensionalized against its value in the inter-plume region at the coronal hole base, so that ρ^0_base (T^0) gives the ratio between the densities (temperatures) on the plume axis and in the background coronal hole. Observed values of ρ^0_base are in the range 3–5. Expression (12) has been chosen following Ahmad & Withbroe (1977), where a gaussian-like density profile is shown to provide the best fit to the observed EUV intensities when the temperature is constant (the same analysis has been applied in X-rays by Ahmad & Webb, 1978). An example of the resulting 2-D density structure near the plume base is shown in Fig. 1, in which the radial decaying behaviour and the conservation of the θ profile at all heights (for a constant temperature) are clearly visible.

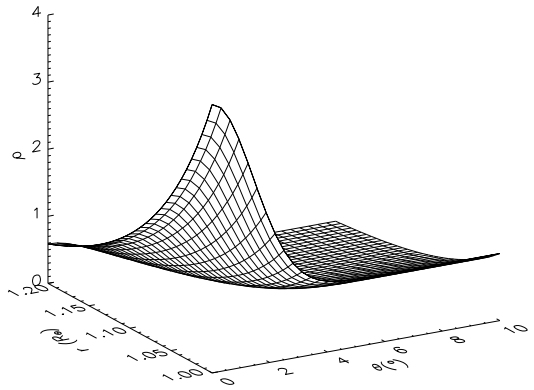

Fig. 1. The density ρ, non-dimensionalized against its value at the base of the coronal hole, as a function of θ and r. The parameters are $\rho^0_{\rm base} = 4$, $T^0 = 1$, $\theta_{\rm w} = 2^\circ$ and $g_\star = 11.5$. Here $\theta_{\rm w}$ is defined as the characteristic angular half width at which the density drops by a factor e^{-1} in respect to the corresponding axial value.

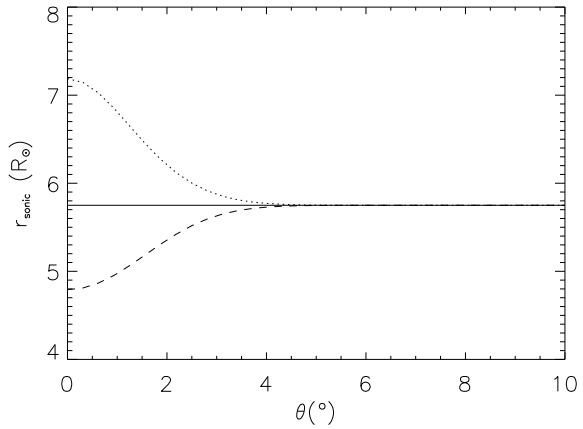

Fig. 2. The position of the sonic point as a function of θ in units of $R_\odot$ (again $\theta_{\rm w} = 2^\circ$ and $g_\star = 11.5$). Three values of $r_{\rm sonic}$ are shown: for T(PL) = T(CH) ($T^0 = 1.0$, solid line), for T(PL) > T(CH) ($T^0 = 1.2$, dashed line) and for T(PL) < T(CH) ($T^0 = 0.8$, dotted line). Note that the sonic point is closer to the Sun for a hot plume and further for a cold plume.

As pointed out earlier, the main effect of a variable temperature is that the sonic point becomes a function of θ, thus affecting also the radial density decay. Assuming a background coronal hole temperature of $T_\star = 10^6\,K$ the resulting sound speed is $V_{s\star} \approx 130\,{\rm km\,s^{-1}}$ and $g_\star = 11.5$. In Fig. 2 the sonic point position is shown as a function of θ for different values of T^0, whereas number density and velocity radial variations are given in Fig. 3 at the plume axis (PL) and for the coronal hole (CH).

Note that the value of the temperature is a crucial parameter for the density and velocity behaviour at large distances. A plume to background temperature ratio as small as $T^0 = 1.2$ implies a variation of $\sim 1\,R_\odot$ in the sonic point position and a density ratio which increases quite rapidly with r. Unfortunately, as Habbal et al. (1993) pointed out in an interesting review of previous observations, temperature measurements in coronal holes are affected by so many unknown parameters (temperature values can only be inferred using some models, where it is usually supposed to be constant across the plume) and uncertain quantities (like element abundances), that the accuracy in the measurements cannot be better than 20%. Therefore, it is obvious that there is no way to deduce our temperature profile in Eq. (13) from observations (there is not even an agreement whether a plume should be cooler or hotter than the surroundings), hence the comparison with observational data in the next sub-section will be done assuming T = const. On the contrary, the present model could be used to calculate the expected emission, for given values of the parameters $T_\star$, T^0, $\rho_\star$, $\rho^0_{\rm base}$ and $\theta_{\rm w}$.

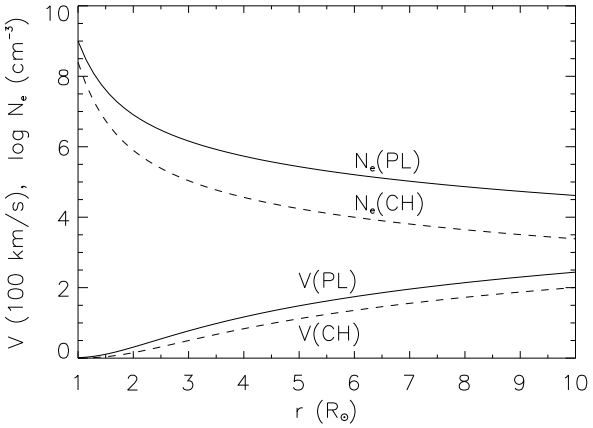

Fig. 3. The number density $N_{\rm e}$ (in units of ${\rm cm^{-3}}$) in logarithmic scale and the velocity V (in units of $100\,{\rm km\,s^{-1}}$). The solid lines refer to the plume axis (PL) whereas the dashed lines refer to the background coronal hole (CH). The parameters are $N_{\rm e}$(PL) = $10^9\,{\rm cm^{-3}}$, $N_{\rm e}$(CH) = $2.5 \times 10^8\,{\rm cm^{-3}}$, T(PL) = 1.2×10^6 K, T(CH) = 10^6 K, $\theta_{\rm w} = 2^\circ$ and $g_\star = 11.5$.

The results shown so far for the radial case may be considered as simple applications of the hydrodynamic theory of isothermal winds, since the magnetic effects have not been taken into account yet. The last step left in our radial case analysis is to calculate the modifications to the zeroth order radial magnetic field, due to the unbalanced pressure gradient across the field lines. In fact, as gravity and inertial forces act radially, Eq. (7) becomes simply

$$\mathscr{L}(A_1) = -r^2 \sin^2\theta \, \frac{\partial P}{\partial A_0},$$

where $\mathscr{L}$ is the operator defined in Eq. (6) and the pressure P has been defined in Eq. (5). Making use of the expressions for ρ and M, the equation for A_1 can be written in the form

$$\mathscr{L}(A_1) \;=\; -r^2 \sin^2\theta \; \rho \left\{ \frac{T}{\rho_{\rm base}} \frac{{\rm d}\rho_{\rm base}}{{\rm d}A_0} + \left[\frac{g_\star}{T} - \frac{1}{2} + \right.\right.$$

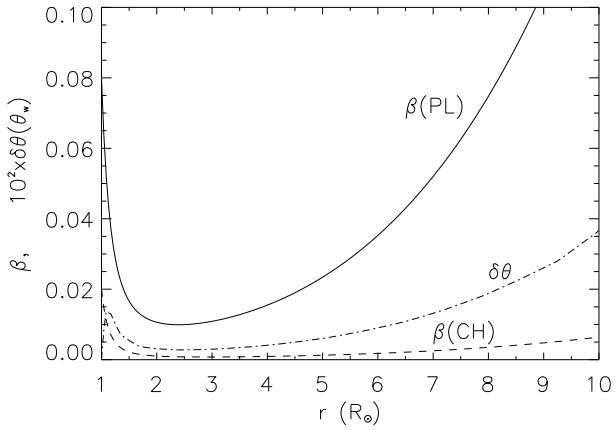

Fig. 4. The plasma beta is shown at the plume axis (PL) and in the coronal hole region (CH) for $\beta_\star = 0.02$. The field line displacement $\delta\theta$ is also shown as a function of r at the plume half width θ_w. The values of the other parameters are the same as in Fig. 3.

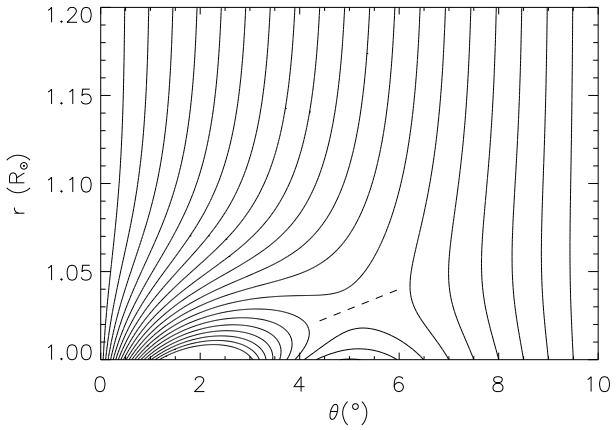

Fig. 5. The field lines of the potential field calculated using Eq. (16) as lower boundary condition. The values of the parameters are $b = 100$ and $\theta_\mathrm{w} = 2.0°$. Since $b > \mathrm{e}^2$, closed structures are present (a large value of b has been chosen in order to enhance the effect). The dashed line indicates the X-point region where a current sheet might form in response to photospheric motions of the bipole.

$$\frac{1}{1-M^2}\left(\ln M + 2\ln\frac{r}{r_\mathrm{sonic}}\right)\right]\frac{\mathrm{d}T}{\mathrm{d}A_0}\Bigg\}, \qquad (14)$$

where the approximation $M^2_\mathrm{base} \ll 1$ has been used. Note that the sonic singularity is removed from the right-hand side thanks to the choice of the arbitrary function $\Psi(A_0)$ corresponding to the transonic solution.

Eq. (14) has been integrated numerically on a square grid $0 \le \theta \le \theta_\mathrm{max}, 1 \le r \le r_\mathrm{max}$ with the condition $A_1 = 0$ on all the boundaries. The solution automatically satisfies the symmetry condition $B_\theta = 0$ at $\theta = 0$. The numerical technique implemented is a linear multigrid solver using a v-cycle (see, for example, Wesseling (1992) for general theory and Fiedler (1992), Longbottom et al. (1996) for specific solar applications of multigrid methods). The multigrid scheme used here results in the expected multigrid behaviour over classical iterative schemes, i.e., the number of iterations to achieve convergence to round off is independent of the number of grid points.

As expected, the modifications to the field lines are very small as long as the condition $\beta \ll 1$ holds, and this also defines the range within which our model retains its validity. In Fig. 4 the plasma beta, both on the plume axis and in the inter-plume region, is plotted together with the angular displacement of the corrected field lines, given by

$$\delta\theta(r,\theta_0) = -\frac{\beta_\star}{2}\frac{A_1(r,\theta_0)}{(\partial A_0/\partial\theta)_{\theta_0}} = -\frac{\beta_\star}{2}\frac{A_1(r,\theta_0)}{\sin\theta_0}.$$

It is interesting to notice that, apart from the line-tying effect at the coronal base (the field lines are supposed to be anchored in the sub-photospheric high-beta plasma), along each field line the behaviour of $\delta\theta$ follows exactly that of the plasma β. This may be seen from a simple dimensional analysis of the equation for A_1, since $A_1/r^2 \sim r^2 P$ and $B_0 = r^{-2}$, thus $\delta\theta \sim A_1 \sim \beta$.

3.2. Flux concentration at the plume base

Although a background radial field is an excellent approximation at large distances, observations show evidence for a super-radial diverging field close to the plume base (see the introduction). As discussed briefly at the beginning of this section, the zeroth order potential field can be modelled by choosing a function $f(\theta)$ giving the non-radial contribution to B_{0r} at the coronal base. A possible choice is

$$f = b(1-\omega)\exp(-\omega); \quad \omega = \frac{1-\cos\theta}{1-\cos\theta_\mathrm{w}} \approx \frac{\theta^2}{\theta_\mathrm{w}^2},$$

where b is a free parameter ($b = 0$ gives the purely radial case) and where the angular width θ_w is chosen to be the same as in Eqs. (12) and (13) ($A_{0\mathrm{w}} \propto 1 - \cos\theta_\mathrm{w}$). Hence, the radial field component and the flux function at $r = 1$ are

$$B_{0r}(1,\theta) \approx 1 + b(1-\theta^2/\theta_\mathrm{w}^2)\exp(-\theta^2/\theta_\mathrm{w}^2), \qquad (15)$$

$$A_0(1,\theta) \approx (\theta^2/2)[1 + b\exp(-\theta^2/\theta_\mathrm{w}^2)], \qquad (16)$$

giving a radial field outside the plume for $\theta \gg \theta_\mathrm{w}$.

Since $f(\theta)$ has a negative minimum at $\theta \approx \sqrt{2}\theta_\mathrm{w}$, where its value is $-b/\mathrm{e}^2$, B_{0r} can be negative if $b > \mathrm{e}^2$, thus giving a region of negative emerging flux around $\sqrt{2}\theta_\mathrm{w}$. In Fig. 5 an example is given with a large value of b. Note that this situation resembles very closely the proposed scenario for plume formation, with close loops interacting with a stronger open flux concentration located at a supergranular junction. The required heating might be provided in the X-point region above the bipole, where a current sheet could form in response to photospheric motions of the bipole.

The main feature of our solution, characteristic of a potential analysis, is that all the modifications to the radial field occur only at low heights, on a scale corresponding to that defined by the

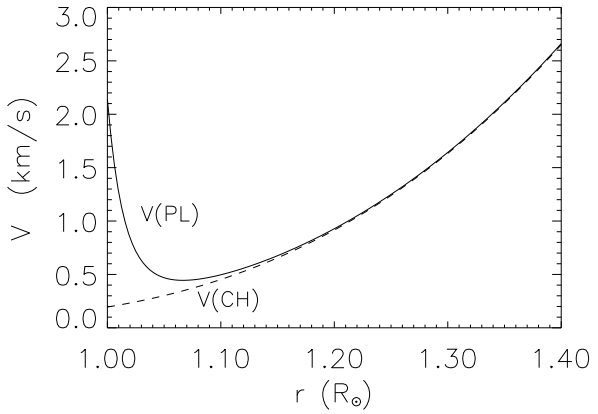

Fig. 6. The flow speed on the axis (solid line) and in the background coronal hole, where the field is radial (dashed line). The modifications due to the non-radial potential field appear only very close to the coronal base, whereas after $\approx 1.2 R_\odot$ the velocity follows exactly the behaviour expected for a purely radial field. The parameters used here are $\rho^0_{\rm base} = 4$, $T^0 = 1$, $b = 10$ and $\theta_{\rm w} = 2.0^\circ$.

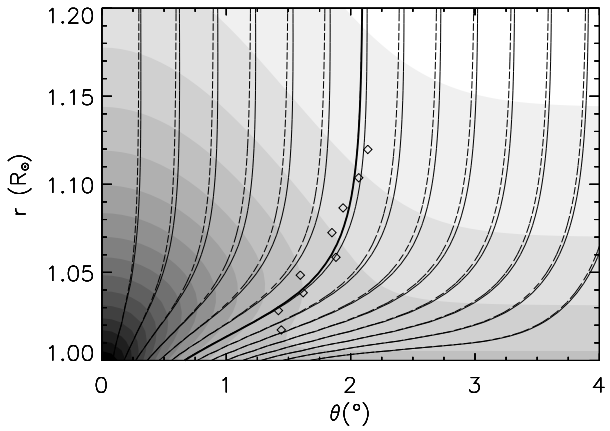

Fig. 7. The corrected field lines (solid), the unperturbed field lines (dashed) and a grey-scale density contour map (denser regions are darker). The thicker line corresponds to the theoretical plume width, defined as the angular distance at which the density drops by a factor e^{-1} with respect to the axial value at the same height, whereas the diamonds are taken from the EUV observations by Ahmad & Withbroe (1977) (the data refers to the NP1 plume in their paper). The parameters used are $\rho^0_{\rm base} = 4$, $T^0 = 1$, $\beta_\star = 0.1$, $b = 10$ and $\theta_{\rm w} = 2.1^\circ$.

plume width: at larger distances the contributions of the higher order multipoles of the photospheric field decay away and the field assumes a radial configuration. This is the same result found by Suess (1982) and the conclusion that can be drawn is that the observed super-radial expansion is indeed due to a magnetic effect, rather than a pressure or inertial one. However, Suess's model does not include any relationship between the density and the magnetic field, necessary to compare the model with the observations, while this comes out quite naturally and in a self-consistent way from our model. Notice that similar results are found in coronal hole models, where the super-radial expansion occurs out to much greater distances (2–3 $R_\odot$, see, for example, Wang & Sheeley, 1990) than in plumes, but where the angular width of the structure is also larger by a corresponding factor.

The best values for the two parameters $\theta_{\rm w}$ and b, which determine the shape of the non-radial potential field through Eqs. (15) and (16), may be obtained by fitting the density structure derived from the theoretical model with some observational data. In order to achieve this, the Bernoulli equation has to be solved numerically for the transonic flow making use of the non-radial, potential background field. However, since the non-radial behaviour is confined to the coronal base, the position of the sonic points remains unaltered and the Mach number is still given by Eq. (10), where now B_0 refers to the general potential solution. The modifications to the velocity are shown in Fig. 6 and these result in a slight enhancement of the flow due to the field concentration at the base.

The density distribution may be still derived from Eq. (11) and the results are shown in Fig. 7, where a contour plot of the density is presented together with the unperturbed (dashed) and corrected (solid) field lines. The density contours are clearly distorted by the field line concentration through the function $\rho_{\rm base}(A_0)$. For a fully isothermal atmosphere ($T^0 = 1$) and neglecting the effects of the flow in the low corona, this function is proportional to the ratio of the density with its axial value at the same height r:

$$\rho(r,\theta)/\rho(r,0) \simeq \rho_{\rm base}[A_0(r,\theta)]/\rho^0_{\rm base},$$

thus providing a means to compare density data with the magnetic field used in the model. In Fig. 7 the thicker solid line refers to a value e^{-1} in the density ratio, defined to be the half angular width of the plume, whereas the diamonds are the observed values taken from the analysis by Ahmad & Withbroe (1977). A good fit appears to be obtained for the values $\theta_{\rm w} = 2.1^\circ$ and $b = 10$.

In spite of the impossibility of deriving with precision the shape of the field lines from the data (a straight line would appear to fit the data just as well!), it is important to remember that observations of plumes taken at larger distances yield a radial behaviour. For example, Fisher & Guhathakurta (1995) found that the density FWHM of polar plumes remains constant in angular width as a function of height extending from 1.16 to 5 $R_\odot$. This observational evidence clearly indicates that the super-radial expansion vanishes on a scale comparable with the width of the plume, thus supporting our potential model.

The modification to the zeroth order field has been worked out by solving directly Eq. (7) and deriving the function Ψ from the knowledge of M and ρ ($M_\star \Psi = \sqrt{T} M \rho / B_0$). Notice that, even for not very small values of the plasma beta ($\beta_\star = 0.1$ in Fig. 7), the corrections to the field lines remain extremely small, thus justifying our method of linearisation with respect to the magnetic field.

4. Conclusions

In this paper an MHD model for solar coronal plumes has been presented. Coronal plumes have been treated as stationary, axisymmetric structures and spherical coordinates have been employed. Since both observational evidence and theoretical investigations seem to agree about the intrinsic magnetic nature of coronal plumes, a linearisation with respect to the magnetic field has been used by assuming a low-beta coronal plasma. This method allows one to decouple the momentum equation components along and across the field lines and to tackle the problem in three distinct steps:

1. The zeroth order potential field is calculated assuming a background radial field and superimposing a non-radial contribution due to a given flux distribution at the plume base.
2. A Bernoulli-type equation is solved for the density along the zeroth order magnetic field lines in the isothermal case. The transonic solution is imposed for the flow along each field line.
3. The modification to the magnetic field, due to the unbalanced forces, is worked out by numerically solving a second order, Poisson-like PDE for the magnetic flux function (transfield or generalised Grad-Shafranov equation).

The method allows for the presence of three free functions, namely the radial field component at the plume base, the density at the plume base and the (constant) temperature along each field line.

In the first part of the work, the plume structure has been considered to be purely radial in order to investigate easily the behaviour of the various physical quantities. The results are obviously what is expected for an isothermal, radial solar wind but with different conditions along each field line. For example, a plume which is hotter than the surroundings shows an increasing ratio of axis to background densities and higher flow speeds (the sonic point occurs closer to the Sun). An original contribution to our radial model is the calculation of the field line displacement due to the unbalanced pressure gradients. This is shown to follow closely the plasma beta behaviour, that is the angular displacement decreases until 2–3 $R_\odot$ and then it increases at larger distances, the only difference being due to the line-tying constraints at $r = R_\odot$ and $r \to \infty$. Obviously, our model retains its validity only until the plasma beta becomes comparable with unity, that is between 10 and 100 $R_\odot$ for typical coronal values, well beyond observational limits.

In the second part the assumption of a purely radial background field has been relaxed by adding to it the contribution due to a flux concentration at the plume base. The resulting potential field shows similarities with that believed to lead to plume formation (closed bipolar loops interacting with a stronger open flux region). However, the main result of our non-radial analysis is the modelling of the observed super-radial expansion near the plume base, through a direct comparison with observational data. The good agreement between the theoretical model and the observations confirms that the plume structure is mainly determined by magnetic effects, whereas pressure and inertial forces only provide higher order perturbations. Another new feature is a slight enhancement in the flow speed (by a few kilometers per second) at the plume's axis and close to the coronal base, due to the concentration of the field lines; however this does not seem to affect the flow at larger distances (the position of the sonic points remains the same as in the radial case).

Future efforts to improve this model will follow three directions: a better modelling of the coronal potential field, allowing for a non-radial plume axis (plumes far from solar poles appear to be bent towards the equator), a more realistic treatment of the plasma energetics, including heat deposition close to the plume base, and possibly the relaxation of the low-beta assumption, thus allowing one to model the behaviour of plumes at large distances from the Sun.

Acknowledgements. The authors wish to thank M. Velli for a critical reading of the manuscript and the referee, Y.-M. Wang, for his useful suggestions.

References

Ahmad I.A., Webb D.F., 1978, Solar Phys. 58, 323
Ahmad I.A., Withbroe G.L., 1977, Solar Phys. 53, 397
Bohlin J.D., Sheeley N.R., Tousey R., 1975, in Space Researh XV, ed. M.J. Rycroft (Akademie – Verlag, Berlin)
Del Zanna L., Chiuderi C., 1996, A&A, 310, 341
Dowdy J.F. Jr., 1993, ApJ 411, 406
Fiedler R.A.S., 1992, in Proc. First SOHO Workshop (ESA SP-348; Noordwijk:ESA), 273
Fisher R., Guhathakurta M., 1995, ApJ 447, L139
Golub L., Krieger A.S., Vaiana G.S., Silk J.K., Timothy A.F., 1974, ApJ 189, L93
Gopalswamy N., Schmahl E.J., Kundu M.R., 1992, in Proc. First SOHO Workshop (ESA SP-348; Noordwijk:ESA), 113
Habbal S.R., 1992, Ann. Geophys. 10, 34
Habbal S.R., Esser R., Arndt M.B., 1993, ApJ 413, 435
Koutchmy S., 1977, Solar Phys. 51, 399
Longbottom A.W., Fiedler R.A.S., Rickard G.J., 1996, Computer Physics Communications (in preparation)
Newkirk G. Jr., Harvey J., 1968, Solar Phys. 3, 321
Parker E., 1958, ApJ 128, 664
Saito K., 1965, PASJ 17, 1
Suess S.T., 1982, Solar Phys. 75, 145
Surlantzis G., Démoulin P., Heyvaerts J., Sauty C., 1994, A&A 284, 985
Surlantzis G., Démoulin P., Heyvaerts J., Sauty C., 1996, A&A 310, 351
Thieme K.M., Marsch E., Schwenn R., 1990, Ann. Geophys. 8, 713
Van de Hulst H.C., 1950, Bull. Astron. Soc. Neth. 11, 150
Velli M., 1994, ApJ 432, L55
Velli M., Habbal S.R., Esser R., 1994, Space Sci. Rev. 70, 391
Walker A.B.C. Jr., Deforest C.E., Hoover R.B., Barbee T.W. Jr., 1993, Solar Phys. 148, 239
Wang Y.-M., 1994, ApJ 435, L153
Wang Y.-M., Sheeley N.R. Jr., 1990, ApJ 355, 726
Wang Y.-M., Sheeley N.R. Jr., 1995a, ApJ 446, L51
Wang Y.-M., Sheeley N.R. Jr., 1995b, ApJ 452, 457
Wesseling P., 1992, An Introduction to Multigrid Methods, John Wiley & Sons LTD
Widing K.G., Feldman U., 1992, ApJ 392, 715